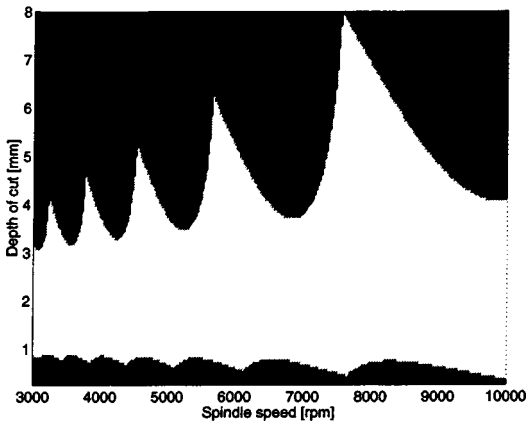

Fig. 3 Stability chart with multiple regions of instability

of cut to near the tool natural frequency at higher depths of cut. As the effective lead angle orients the thrust force more orthogonal to a vibration mode, the mode's contribution to the vibration of the system is reduced. In the limiting case, it will reduce the two degree of freedom system to a one degree of freedom system. For such a system at low spindle speeds (relative to modal natural frequencies), it is well known that the chatter frequency will be near the natural frequency of the single mode. For the given two degree of freedom system, at low depths of cut the effective lead angle orients the thrust force more along the transverse direction of the workpiece (perpendicular to feed direction). At higher depths of cut, the effective lead angle approaches the side cutting edge angle of the tool, which, in this case, orients the force more along the transverse direction of the cutting tool (feed direction). In these two cases, the system may be modeled as a one degree of freedom in the X direction (at low depths of cut) and a one degree of freedom system in the Z direction (at higher depths of cut). Therefore, it is expected that the chatter frequency would be near the workpiece natural frequency at low depths of cut and near the tool natural frequency at high depths of cut.

The effect of the nose radius on the lower limit of stability is clearly seen by comparing case 1 to case 2 and by comparing case 3 to case 4 in Fig. 1. The upper limit of stability is unaffected by the change in nose radius but the lower limit changes. As the nose radius increases, the lower limit of stability increases. This follows directly from the fact that the influence of the nose radius on the effective lead angle continues to a larger depth of cut for a larger value of the nose radius.

5 Improved Stability Chart

This nonlinear influence of the effective lead angle changes the look of the stability charts for many processes involving cutting with a corner radiused tool. An example stability chart generated with the approach explained in this paper is presented in Fig. 3. The unstable regions of the cutting process are represented in the figure with the shading and the stable regions are white. Two key features of this modified stability chart can be seen. First, there exists an envelope in which the process is stable as opposed to just an upper limit on the depth of cut for a stable process. Second, since the important structural frequency is different at low depths of cut than at higher depths of cut, the peaks on the lobes at high depth of cut are located at different spindle speeds than the lower limit of the low depth of cut limit. For example, there is a peak in the upper limit at 5700 rpm while the valley of the lower limit has its minimum near 6100 rpm.

6 Conclusion

From this work, the following conclusions can be made

- By linearizing the characteristic equation at every depth of cut, multiple regions of stability can be predicted.
- The multiple regions of stability are caused by the changing effective lead angle aligning the thrust force in different directions as the depth of cut is increased.
- By reducing the nose radius of the insert, the lower limit of the envelope of stability seen for turning systems of long, slender bars can be reduced.

7 Acknowledgment

This research was supported by the Ford Motor Company and the National Science Foundation Industry/University Cooperative Research Center for Machine Tool Systems Research at the University of Illinois at Urbana-Champaign.

References

[1] Merritt, H. E., 1965, ''Theory of Self-Excited Machine Tool Chatter,'' ASME J. Eng. Ind., **87**, pp. 447–454.
[2] Tlusty, J., and Polacek, M., 1963, ''The Stability of the Machine Tool Against Self-Excited Vibration in Machining,'' International Research in Production Engineering, pp. 465–474.
[3] Ozdoganlar, O. B., and Endres, W. J., 1998, ''An Analytical Stability Solution for the Turning Process with Depth-Direction Dynamics and Corner-Radiused Tooling,'' *Proceedings of the ASME Symposium on Advances in Modeling, Monitoring, and Control of Machining Systems*, **DSC-64**, pp. 511–518.
[4] Rao, B. C., and Shin, Y. C., 1999, ''An Comprehensive Dynamic Cutting Force Model for Chatter Prediction in Turning,'' Int. J. Mach. Tools Manuf., **39**, pp. 1631–1654.
[5] Ozdoganlar, O. B., and Endres, W. J., 1997, ''A Structured Approach to Analytical Multi-Degree-of-Freedom Time-Invariant Stability Analysis for Machining,'' *Proceedings of the ASME Symposium on Predictable Modeling in Metal Cutting as Means of Bridging the Gap Between Theory and Practice*, **MED-6-2**, pp. 153–160.
[6] Fu, H. J., DeVor, R. E., and Kapoor, S. G., 1984, ''A Mechanistic Model for the Prediction of the Force System in Face Milling Operations,'' ASME J. Eng. Ind., **106**, pp. 81–88.
[7] Endres, W. J., and Waldorf, D. J., 1994, ''The Importance of Considering Size Effect Along the Cutting Edge in Predicting the Effective Lead Angle for Turning,'' Transactions of the NAMRI/SME, **22**, pp. 65–72.

Experimental Investigation of Polymeric Material Removal by Low Diffraction Laser Beam

Xuanhui Lu

Y. Lawrence Yao
e-mail: YLY1@columbia.edu

Kai Chen

Department of Mechanical Engineering, Columbia University, 220 Mudd Bldg., MC 4703, New York, NY 10027

Effects of improved beam quality of a low diffraction laser beam on laser material removal processes are experimentally investigated in a polymeric material. The experimental results are in agreement with theoretical predictions. The results show that the low diffraction beam has marked advantages over the Gaussian beam in ablation-dominated material removal processes in terms of larger depth and smaller taper at the same average power level. [DOI: 10.1115/1.1445156]

Contributed by the Manufacturing Engineering Division for publication in the JOURNAL OF MANUFACTURING SCIENCE AND ENGINEERING. Manuscript received November 1999; Revised February 2001. Associate Editor: S. Smelser.

1 Introduction

Laser beam quality plays an important role in quality and efficiency of laser materials processing applications. Higher beam quality typically means nearly fundamental-mode oscillation. Many efforts have thus been made to change high-order modes into the fundamental modes including simple methods such as using an aperture but often at the cost of excessive power attenuation. The fundamental-mode Gaussian beam (i.e., TEM_{00}-Transverse Electromagnetic Mode) has long been regarded as an ideal beam, or diffraction-limited beam. The beam quality can be described quantitatively in term of M^2 as defined by Siegman [1]. A product of the standard deviation of the beam size and that of the divergence is formed. M^2 is the ratio of the product for a non-diffraction-limited, multi-transverse-mode beam, to that of a Gaussian beam. The M^2 for the fundamental-mode Gaussian beam is thus unity. An interesting question is whether or not it is possible for a practical beam to have an M^2 value smaller than that of the fundamental-mode Gaussian beam. The concept of a low-diffraction beam having $M^2<1$ has been proposed [2,3]. The low diffraction beam is based on the boundary diffraction principle. An advantage of the beam is that it can be obtained by altering the existing resonator of a CO_2 laser through a special phase plate implemented at the resonator rear mirror (Fig. 1). Additional details can be founded in [2,3].

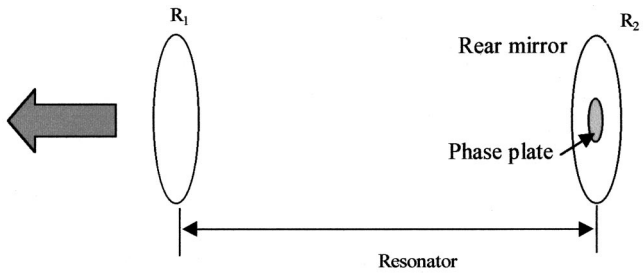

Fig. 1 Schematic of resonator configuration (with a half phase plate attached on the rear mirror inside laser cavity) to realize the low diffraction beam

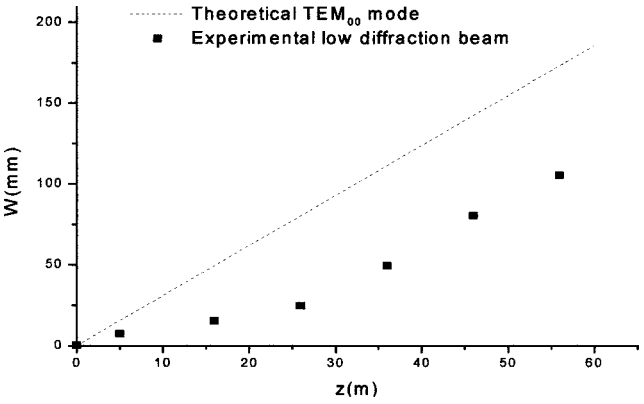

Fig. 2 Beam radius of the measured low diffraction beam and theoretical TEM_{00} mode vs. axial distance between the output coupler to the measurement location

The next question is whether the low-diffraction beam, whose M^2 value is smaller than that of a Gaussian beam, will translate into better quality and efficiency in laser materials processing applications, such as laser machining. Although it is generally agreed that the laser beam quality has a direct effect on machining quality, no consensus has been reached that a smaller M^2 is always beneficial to a machining process because the machining process is a complicated thermal process that could also involve fluid flow and melt rejection. A beam with a smaller M^2 value is likely to result in smaller hole sizes or narrower slots, which is not in favor of melt rejection. However, in an ablation-dominated laser machining process, most of the material is vaporized almost instantly and is mainly removed by vapor pressure. The low diffraction laser beam with a smaller M^2 value is thus expected to have beneficial effects on the ablative machining process.

The quality and profile of laser made holes, grooves and cuts are obviously of importance especially in the growing microelectronic and precision medical device industry [4–6]. The quality is generally gauged by wall definition, extent of heat-affected zone, and ability to produce features with higher aspect ratio. Laser ablation of polymeric materials using laser beams is a well-established process and examples are found in [7,8]. Factors of laser beams likely to affect drilling and grooving have been studied in many reports [9,10]. This paper presents the application of a low diffraction beam to ablation-dominated drilling and grooving processes involving a polymer material. Its beneficial effects on process quality are investigated in comparison with a Gaussian beam.

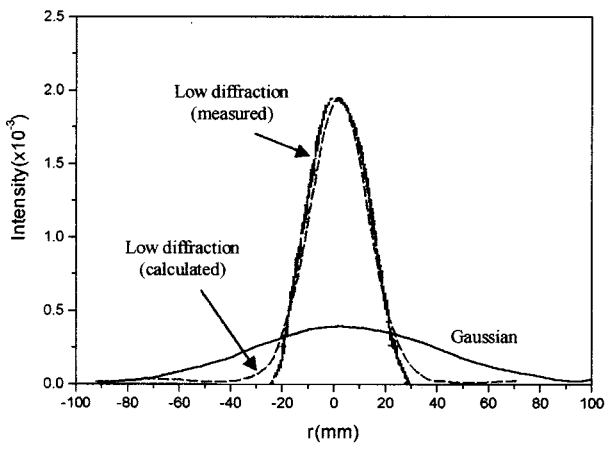

(*a*) Far field

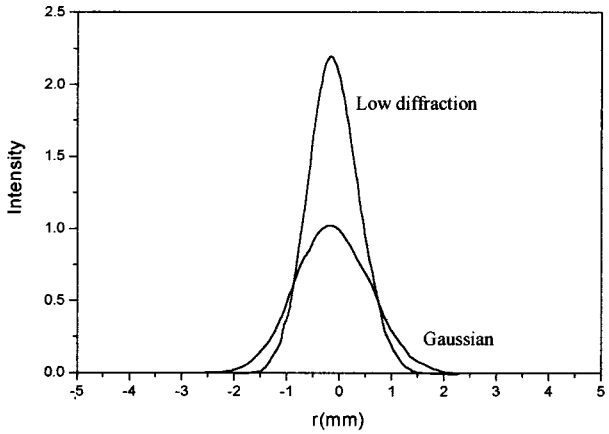

(*b*) Near field

Fig. 3 Intensity distributions (calculations are based on Eqs. (2) and (3), with $W_0=1.49$ mm (experimentally measured) and $M_e^2=0.3$ (using Eq. (1)))

2 Characterization of the Low Diffraction Beam

Experiments were carried out using a continuous-wave CO_2 laser with maximum average power of 12 W. The original resonator of the laser system generates a fundamental mode Gaussian beam (i.e., TEM_{00}). According to the principle described in [2,3], an identical resonator is modified with its structure as schematically shown in Fig. 1 to generator a low diffraction beam. The intensity profile and divergence of beams from both resonators were measured. Because the output of the low diffraction beam is not a Gaussian distribution, it is more practical to use the definition of 86.5 percent power content to measure the beam size. In order to compare the beam quality of this new mode with the Gaussian mode, the equivalent beam quality factor M_e^2 is defined as follows:

$$M_e^2 = W_{86.5}\theta_{86.5}\frac{\pi}{\lambda} \tag{1}$$

where $W_{86.5}$ is the equivalent beam waist size with 86.5 percent power content, $\theta_{86.5}$ is the divergence angle corresponding to the 86.5 percent power content, and λ is the beam wavelength.

The intensity distribution of Gaussian beam $I_0^G(r)$, and the low diffraction beam, $I_0^L(r)$ at the beam waist can be written as

$$I_0^G(r) = I_0 \exp\left(-\frac{2r^2}{W_0^2}\right)$$
$$I_0^L(r) = I_0 \exp\left(-\frac{2r^2}{W_0'^2}\right) = I_0 \exp\left(-\frac{2r^2}{M_e^2 W_0^2}\right) \tag{2}$$

where W_0 is the Gaussian beam waist radius and I_0 is the peak intensity. The intensity distribution at the far field can be obtained by using the beam propagation law, i.e., *ABCD* law [11]:

$$I_z^G(r,z) = I_1 \exp\left[\frac{-2r^2}{W_0^2(1+z^2/z_r^2)}\right]$$
$$I_z^L(r,z) = I_2 \exp\left[\frac{-2r^2}{W_0'^2(1+z^2/z_r^2)}\right]$$
$$= I_2 \exp\left[\frac{-2r^2}{M_e^2 W_0^2(1+z^2/z_r^2)}\right] \tag{3}$$

where z is the axial distance from the waist, and $z_r = \pi W_0^2/\lambda$ is the Rayleigh range.

The focal point radius for a Gaussian beam, W_f^G, is well known [12]:

$$W_f^G = \frac{\lambda}{\pi W_z} \tag{4}$$

where λ is wavelength, f is lens focal length, and W_z is original unfocused beam radius. The depth of focus for a Gaussian beam, h_G, is briefly derived below.

According to Gaussian beam properties, its beam radius, at any distance along the beam path, z, from the waist is given from the basic propagation equation:

$$W(z) = W_0\left[1+\left(\frac{z}{z_r}\right)^2\right]^{1/2} \tag{5}$$

The depth of focus is normally defined as the distance between two points slightly away from the beam waist and the beam radius at these points is about 5 percent above the beam waist radius. By substituting $W(z) = 1.05\ W_0$ into Eq. (5), the depth of focus is obtained as:

$$h_G = \frac{0.64\lambda}{\pi}\left(\frac{f}{W_z}\right)^2 \tag{6}$$

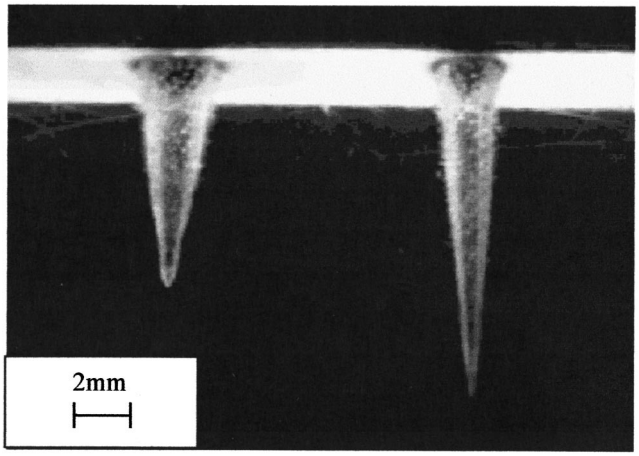

Fig. 4 Acrylic imprints with Gaussian (left) and the low diffraction beam (right) (9W, 1 sec, both unfocused)

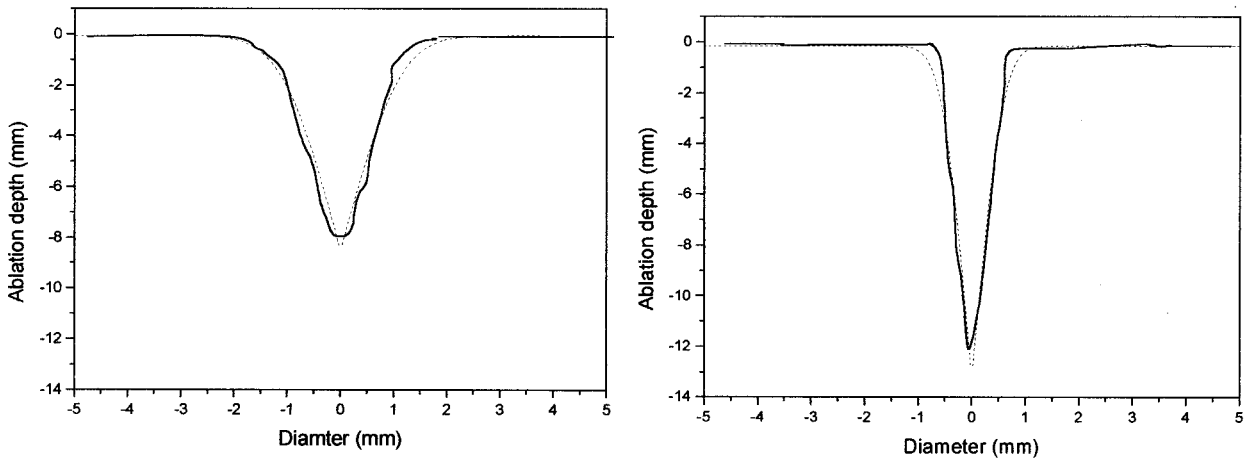

(*a*) With Gaussian beam (*b*) With the low diffraction beam

Fig. 5 Theoretical (dotted line) and experimental results (solid line) of hole profiles (power=9 W, duration=1 sec, unfocused, acrylic)

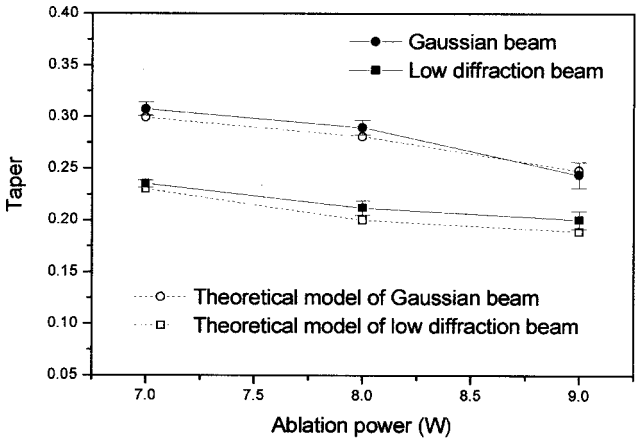

Fig. 6 The hole taper vs. ablation power (ablation duration = 0.8 sec, focused, acrylic)

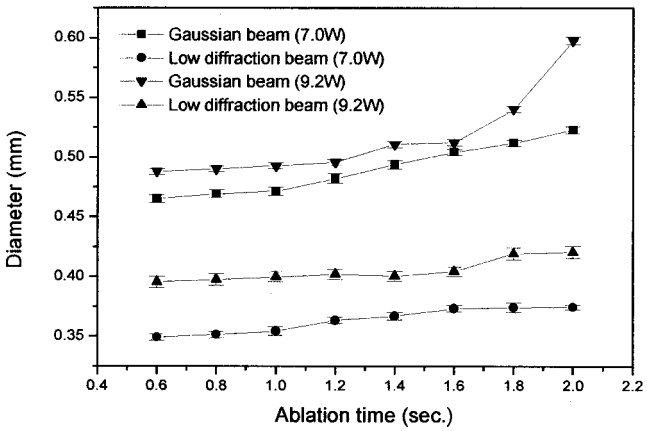

Fig. 8 Drilled hole diameter comparison between the Gaussian beam and the low diffraction beam vs. ablation time (focused, acrylic)

According to the M_e^2 definition (Eq. 1), the focal point radius of a low diffraction beam of M_e^2 can be written as follows.

$$W_f^L = \frac{M_e^2 \lambda f}{\pi W_z} \tag{7}$$

For the low diffraction beam, its Rayleigh range $z_r = \pi W_0^2 / M_e^2 \lambda$. Then the focal depth of the low diffraction beam can be approximately represented as:

$$h_L = \frac{0.64\lambda}{\pi M_e^2} \left(\frac{f}{W_z} \right)^2 \tag{8}$$

Compared to the focal point radius and the focal depth of a Gaussian Beam, i.e., Eq. (4) and Eq. (6), the focal point radius for the low diffraction beam is smaller than that of the Gaussian beam, while the focal depth for the low diffraction beam is larger than that of the Gaussian beam, since the M_e^2 value for the low diffraction beam is less than unity.

Figure 2 shows experimental results of beam radius of the low diffraction beam at various distances. It is seen that the divergence angle of the low diffraction beam is smaller than that of theoretical TEM_{00} mode. Based on experimentally measured $W_{86.5}$ and $\theta_{86.5}$, and $\lambda = 10.6\ \mu$m for the CO_2 laser, the equivalent beam quality factor $M_e^2 \cong 0.3$ is obtained.

The intensity profile of the low diffraction beam in the far field is experimentally measured and superposed in Fig. 3(*a*) with the calculated intensity profiles of both the low diffraction and Gaussian beam according to Eq. (3). As seen, there is a good agreement between the experimental and calculated profiles, and the low diffraction beam has a much higher central intensity and smaller divergence than that of the Gaussian beam. Using Eq. (2), the near-field intensity profiles of both beams are plotted in Fig. 3(*b*). It can be seen that the low diffraction beam in the near field also has higher central intensity and smaller diameter than the Gaussian beam.

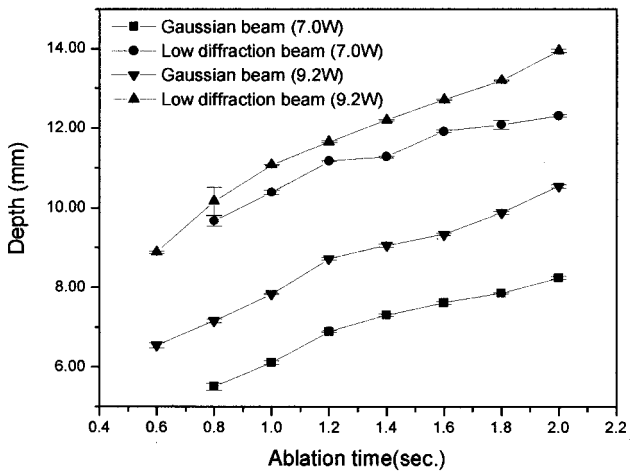

Fig. 7 Drilling depth comparison between the Gaussian beam and the low diffraction beam vs. ablation duration (focused, acrylic)

3 Comparison of Theoretical and Experimental Results

Figure 4 shows imprints made on acrylic by the Gaussian beam (best achievable on the laser used) and low diffraction beam (both unfocused) when the average power is 9 W. Acrylic is chosen primarily because of its low ablation threshold that the laser used can reach. It is also because its removal is primarily due to ablation such that the imprint better reflects the beam shape. Although the power level is the same, the low-diffraction beam has a higher energy intensity and a smaller beam size. Not surprisingly, the hole profiles closely follow that of beams in the ablative machining process. Cross-sections of the profiles are also shown in solid lines in Fig. 5 to compare with a theoretically calculated ablation profiles shown in dotted lines.

The theoretically calculated ablation profiles are obtained based on the model by Andrews and Atthey [13]. The energy density and the beam size for both the low diffraction beam and Gaussian beam are experimentally obtained and used in the theoretical model to predict the hole profile as shown in Fig. 5 in dotted lines. The waist radius for the resonator generating the Gaussian beam is measured as $W_0 = 1.49$ mm, while for the resonator generating the low diffraction beam the beam radius is measured as $W_0' = 0.75$ mm. As a result, the intensity is 129 W/cm^2 at the waist for the Gaussian beam, and 509 W/cm^2 at the waist for the low diffraction beam. The theoretical predication agrees with experimental results.

There is some discrepancy at the top part of the hole profiles under the condition of the low diffraction beam (Fig. 5(*b*)). The reason is that beam intensity in the theoretical model is based on

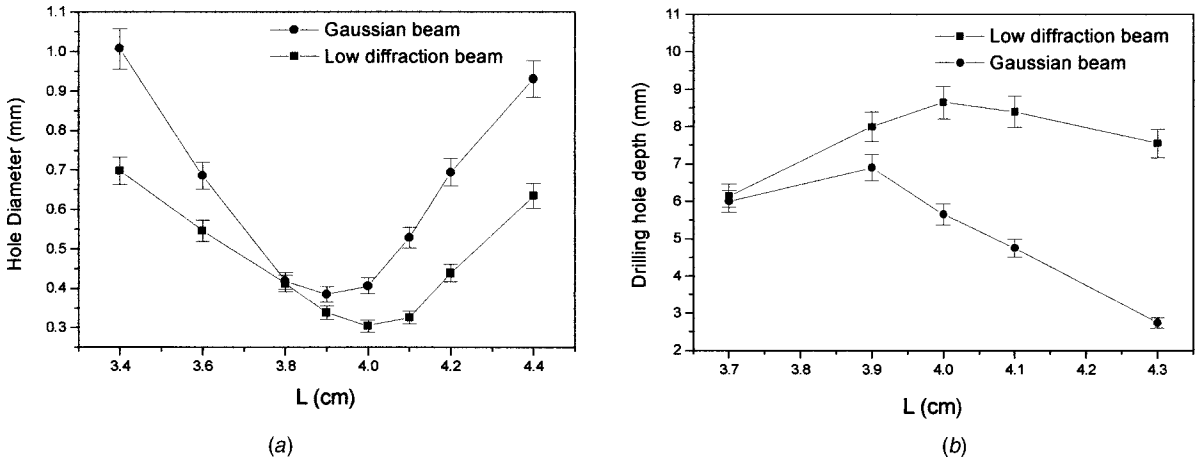

Fig. 9 (a) Hole diameter and (b) depth vs. the distance from focus lens to workpiece top surface (focal length =4 cm, power=7 W, duration=0.5 sec)

a deformed Gaussian beam of optical beam quality factor M_e^2, while the actual beam is obtained based on the boundary diffraction principle.

The beams are then focused using a lens with a focal length of 40 mm. The CO_2 laser varies at two average power levels, 7 W and 9.2 W. For the Gaussian beam, the resultant average power intensity is 5.22×10^4 W/cm^2 for 7 W, and 6.71×10^4 W/cm^2 for 9.2 W. For the low diffraction beam, the resultant average power intensity is 2.01×10^5 W/cm^2 for 7 W, and 2.68×10^5 W/cm^2 for 9.2 W.

Figure 6 shows the variation of hole taper against ablation power for both the low diffraction beam and Gaussian beam. Taper is defined as the ratio of hole diameter to hole depth (therefore is the inverse of aspect ratio) and is one of the quality factors for hole profile. It is seen from Fig. 6 that the hole drilled with the low diffraction beam has significantly smaller taper values than the hole drilled with Gaussian beam. The predicted values from the theoretical model are also shown in the figure and are generally in agreement with the measured values. The taper value decreases with the increasing power level for both low diffraction beam and Gaussian beam. This is because the diameter of the hole increases much slower than the hole depth when the power level increases, as seen from Figs. 7 and 8.

4 Parametric Studies and Grooving Experiments

Figure 7 shows the measured drilling depth vs. ablation time at two power levels. The hole depth drilled with the low diffraction beam is much larger than that with the Gaussian beam because of the higher central energy intensity at the same average power level. The depth with the low diffraction beam is about 40 percent higher than that with the Gaussian beam under the condition used.

Figure 8 shows the measured diameter of the drilled hole vs. ablation time at two power levels. It is seen that the hole diameter drilled with low diffraction beam is about 25 percent smaller than that with Gaussian beam. In addition, with the ablation time increasing, the drilled hole diameter with the low diffraction beam increases slower than that with the Gaussian beam especially at longer ablation times clearly because the low diffraction beam has smaller divergence and longer focal depth. The parametric studies confirm that the low diffraction beam consistently provides better results under different laser power and ablation time. Power levels of 7 W and 9.2 W were used to avoid to be too close to the maximal power of the laser used (12 W) but be high enough to remove the material.

Equations (6) and (8) show that the low diffraction beam has a longer depth of focus than that of a Gaussian beam because M_e^2

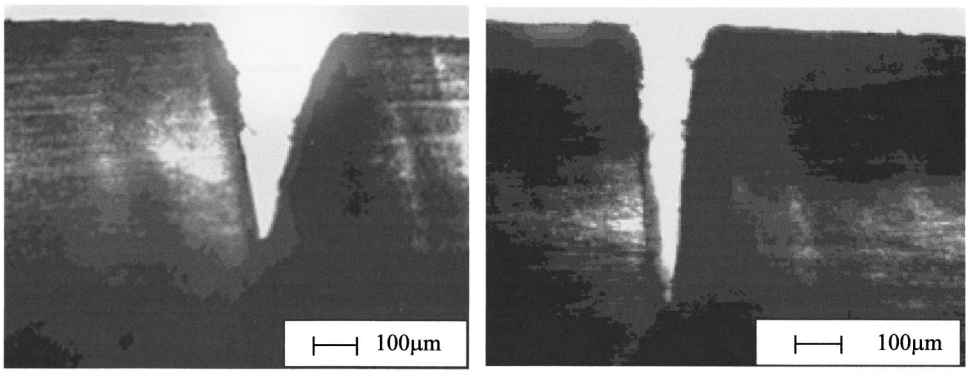

Fig. 10 Typical groove profiles with Gaussian beam and the low diffraction beam (power =9 W, speed=14 mm/sec, both focused, acrylic)

<1 for the low diffraction beam. As seen in Fig. 9(*a*), the hole diameter drilled with the low diffraction beam and the Gaussian beam change from about 0.3 to 0.7 mm and 0.4 to 1.0 mm, respectively, when the distance L between the focus lens to top surface of the workpiece are changed from 3.4 to 4.4 cm (the focal length of the lens is 4 cm). This verifies that the low diffraction beam has a longer depth of focus. Obviously, when L is around 4 cm, the focal point which has the minimal beam diameter is right on the top surface of the workpiece. As a result, the hole diameter is the smallest when Li is around 4 cm. From Fig. 9(*b*), it is seen that the hole depth varies slower for the low diffraction beam than for the Gaussian beam when L is around 4 cm. The longer depth of focus of the low diffraction beam is desirable especially when thick section machining is concerned.

The focused low diffraction beam and Gaussian beam are applied to grooving the same material. Figure 10 compares the cross sections of groove profiles ablated by both beams. It is seen that at the same power level (9 W) and the grooving speed (14 mm/s), the cross sectional profile with the low diffraction beam has a lower taper or higher aspect ratio than that with the Gaussian beam. It is seen that the beneficial effects of the low diffraction beam in drilling extend to applications such as grooving and likely cutting as well. These beneficial effects include a higher aspect ratio and lower sensitivity to focal point location. They are expected to be more significant at higher power levels. While this paper only covers acrylic, other materials are expected to have similar beneficial effects when ablated by the low diffraction beam because during ablative laser machining, machined profiles chiefly rely on the optical beam quality. When the power intensity is below the ablation threshold of a material, other factors also play a significant role.

5 Conclusion

A low diffraction beam, which has a M^2 factor smaller than unity, is implemented with a low power CO_2 laser and applied to ablation-dominated drilling and grooving of acrylic. The experimental results show that the low diffraction beam produced larger depth, smaller taper and smaller hole diameter, as compared with a Gaussian beam at the same average power level. This holds true for both the unfocused and focused cases. The depth of focus of the focused low diffraction beam is also longer than the Gaussian beam, indicating its suitability for processing thick sections of material. Similar results are obtained when the beam is applied to grooving applications. If the implementation of the low diffraction beam is extended to a higher power level laser system, the above mentioned beneficial effects will be more significant. For other materials, as long as ablation is the dominant mechanism of material removal, similar beneficial effects can be expected. In cases where ablation is not dominant, the low diffraction beam is likely to offer at least some of the advantages but further studies are needed.

Acknowledgments

The financial support provided via a Pao Scholarship and Columbia University is gratefully acknowledged.

References

[1] Siegman, A. E., 1993, "Defining and Measuring Laser Beam Quality," *Solid State Laser-New Developments and Applications*, M. Inguscio and R. Wallenstein, eds., Plenum, New York, pp. 13–28.
[2] Wang, S., Lu, X., Pan, C., and Yu, S., 1995, "A New Beam CO_2 Laser," Optik (Stuttgart), **101**, pp. 32.
[3] Wang, S. et al., 1995, "A New Beam Produced by CO_2 laser," Optik (Stuttgart), **101**, pp. 84.
[4] Yibas, B. S., 1987, "Study of Affecting Parameters in Laser Hole Drilling of Sheet Metals," ASME J. Eng. Mater. Technol., **109**, pp. 282–287.
[5] Olson, R. W., and Swope, W. C., 1993, "Laser Drilling with Focused Gaussian Beams," J. Appl. Phys., **72**, No. 8, pp. 3686–3696.
[6] Rohde, H., and Dausinger, F., 1995, "The Forming Process of a Through Hole Drilled with a Single Laser Pulse," *ICALEO'95*, pp. 331–340.
[7] Miyamoto, I., and Maruo, H., 1991, "The Mechanism of Laser Cutting, Welding in the World," Journal of the International Institute of Welding, **29**, No. 9/10, pp. 283–294.
[8] Redmond, T. F., Lankard, J. R., Balz, J. R., Proto, G. R., and Wassick, T. A., 1993, "The Application of Laser Process Technology to Thin Film Packaging," IEEE Trans. Compon., Hybrids, Manuf. Technol., **16**, No. 1, pp. 6–12.
[9] Batteh, J. J., Chen, M. M., and Mazumder, J., 1998, "Scaling and Numerical Analysis of Pulsed Laser Drilling," *ICALEO'98*, B-30.
[10] Powell, J., 1993, *CO_2 Laser Cutting*, Springer-Verlag.
[11] Kogelnik, H., and Li, T., 1966, "Laser Beams and Resonators," Appl. Opt., **5**, pp. 1550.
[12] Collins, S. A., 1970, "Lens-System Diffraction Integral Written in Term of Matrix Optics," J. Opt. Soc. Am., **60**, No. 9, pp. 1168–1177.
[13] Andrews, J. G., and Atthey, D. R., 1976, "Hydrodynamic Limit to Penetration of a Material by a High-Power Beam," J. Phys. D, **9**, pp. 2181–2194.

Design of Reconfigurable Machine Tools

Yong-Mo Moon
Research Fellow
e-mail: ymmoon@engin.umich.edu

Sridhar Kota
Professor
e-mail: kota@engin.umich.edu

Dept. of Mech. Engr., NSF Engineering Research Center for Reconfigurable Machining System, University of Michigan, Ann Arbor, MI 48109-2125

In this paper, we present a systematic methodology for designing Reconfigurable Machine Tools (RMTs). The synthesis methodology takes as input a set of functional requirements—a set of process plans and generates a set of kinematically viable reconfigurable machine tools that meet the given design specifications. We present a mathematical framework for synthesis of machine tools using a library of building blocks. The framework is rooted in (a) graph theoretic methods of enumeration of alternate structural configurations and (b) screw theory that enables us to manipulate matrix representations of motions to identify appropriate kinematic building blocks. [DOI: 10.1115/1.1452748]

Introduction

A Reconfigurable Machine Tool (RMT) is designed to process a given family of machining features and is constructed from a set of standard modules. An RMT provides a cost-effective solution to mass customization and high-speed capability. There is no known systematic method or a scientific basis for designing RMTs [1]. This paper presents a mathematical framework for design of RMTs starting from process requirements. The key feature of this methodology is the use of screw-theory based mathematical representation to transform a given description of machining tasks to be performed (process planning data) into a machine tool that is capable of performing the prescribed machining tasks. Starting from machining operations data, a set of feasible structural configurations of the machine is determined using graph theory. Various machine functions are then mapped to individual entities in each structural configuration. Using a precompiled parameterized

Contributed by the Manufacturing Engineering Division for publication in the JOURNAL OF MANUFACTURING SCIENCE AND ENGINEERING. Manuscript received Jan. 1999; Revised Aug. 2001. Associate Editor: K. Ehmann.